Fabrication, characterization and studies of annealing effects on ferromagnetism in $Zn_{1-x}Co_xO$ nanowires

2006 Nanotechnology 17 5511

(http://iopscience.iop.org/0957-4484/17/21/036)

INSTITUTE OF PHYSICS PUBLISHING NANOTECHNOLOGY
Nanotechnology **17** (2006) 5511–5518 doi:10.1088/0957-4484/17/21/036

Fabrication, characterization and studies of annealing effects on ferromagnetism in $Zn_{1-x}Co_xO$ nanowires

Z Y Wu[1], F R Chen[1], J J Kai[1], W B Jian[2,4] and J J Lin[2,3,4]

[1] Department of Engineering and System Science, National Tsing Hua University, Hsinchu 300, Taiwan
[2] Department of Electrophysics, National Chiao Tung University, Hsinchu 300, Taiwan
[3] Institute of Physics, National Chiao Tung University, Hsinchu 300, Taiwan

E-mail: wbjian@mail.nctu.edu.tw and jjlin@mail.nctu.edu.tw

Received 9 June 2006, in final form 3 October 2006
Published 20 October 2006
Online at stacks.iop.org/Nano/17/5511

Abstract
Diluted magnetic semiconductor $Zn_{1-x}Co_xO$ ($x \leqslant 0.11$) nanowires with average diameter of ~40 nm were prepared by thermal evaporation, followed by high-energy Co ion implantation. Bombardment by Co ions produced a good number of structural defects (stacking faults and orientational variations) in the nanowires. The as-implanted nanowires were paramagnetic. We performed two types of thermal annealing, one in 1 atm argon flow and the other in a high vacuum, at 600 °C, and studied the effects of annealing on the magnetic properties of these nanowires. Argon annealing removed structural defects in the nanowires and the nanowires then revealed ferromagnetic ordering. This result suggests that structure defects are harmful to the occurrence of ferromagnetism in the Co-implanted ZnO. The structure of the as-implanted and the annealed nanowires was inspected in detail by using scanning electron microscopy, energy dispersive x-ray spectroscopy, maps of electron energy loss spectra, x-ray diffraction, and high-resolution transmission electron microscopy. Taken together, these studies suggested that no second phase existed on the scale down to the spatial resolution of ~0.5 nm. Noticeably, the nanowires even displayed largely enhanced ferromagnetism after annealing in a high vacuum. A subsequent annealing in oxygen has also been performed on those vacuum-annealed nanowires to study the roles played by the O vacancies in determining the ferromagnetic properties of the nanowires. Our results indicate that both the improved structural quality and the increased number of O vacancies are key factors for the occurrence of ferromagnetic ordering in the $Zn_{1-x}Co_xO$ nanowires.

1. Introduction

Diluted magnetic semiconductors [1] (DMSs) have attracted much attention because of the possibility of introducing the spin degree of freedom into the charge controllable semiconductor devices. The integration of charge and spin in the existing semiconductor technologies, such as transistor, memory, and magnetic recording technologies, has evolved into a new field of fundamental and applied research called 'spintronics' [2]. A DMS is known to be a good candidate for the application of spintronic devices and scientists are searching for room-temperature (RT) ferromagnetic DMSs. An experimental result of the influence of carrier concentration on ferromagnetism (FM) of the IV–VI DMS material, PbSnMnTe, was reported [3] and indirect exchange via the Ruderman–Kittel–Kasuya–Yosida (RKKY) interaction was proposed to explain the occurrence of the observed FM. The transition temperature of the IV–VI DMS material was, however, too low to be useful in real applications. Munekata

[4] Authors to whom any correspondence should be addressed.

et al [4] demonstrated the existence of FM in the III–V DMS $In_{1-x}Mn_xAs$. Afterwards the new III–V DMS of (Ga, Mn)As was prepared and it was found to have a Curie temperature (T_C) as high as 110 K [5, 6]. Recently, Dietl *et al* [7] have theoretically explained the 110 K high T_C found in the p-type DMS of (Ga, Mn)As. Furthermore, they have predicted the possible existence of RT FM in GaMnN and ZnMnO. The above-mentioned works have recently triggered intense research activities on DMS materials, both theoretical and experimental.

ZnO is a II–VI DMS host material with a wurtzite structure. It possesses a direct, wide band gap of ∼3.3 eV and a large exciton binding energy of ∼60 meV. ZnO is transparent and can be over-doped to form conductive films [8, 9] for applications in the display technology. ZnO-based materials are expected to be widely used in optoelectronics [10], solar cells, gas sensors, and nanoelectronic devices in the near future [11]. Co-doped ZnO stands out as one of the possible candidates for RT FM. Experimentally, Ueda *et al* [12] and several groups [13–20] have suggested RT or intrinsic FM in Co-doped ZnO films, while other groups have reported either the absence of FM or even the presence of antiferromagnetism [21, 22]. Other groups have argued for extrinsic FM [23] due to the existence of second phases of Co nanocrystals [24, 25] and microstructures [26]. Theoretically, a double-exchange mechanism either from the Zener model description [7] of delocalized high-density carriers inducing RKKY-like interactions or from the transition metals resulting in deep impurity band states [27, 28] has been proposed to explain the FM in $Zn_{1-x}Co_xO$. The indirect exchange via donor defects and bound magnetic polarons [29, 31] was argued to explain the high Curie temperatures in dilute FM oxides. Theoretical models of both n-type [30, 31] and p-type doping [32, 7] have been given to realize RT FM in ZnO-based DMS.

Nanowire structures of ZnO-based DMSs with diameters smaller than 100 nm, which is a typical thickness of the specimen usually used for transmission electron microscopy (TEM) studies, provides a new platform to study structure effects on physical properties. It is known that different growth conditions, atomic structures (e.g., being crystalline or polycrystalline), and thermal annealing conditions can lead to distinct magnetic properties of Co-doped ZnO. Thus, in this work we performed thermal annealing on our $Zn_{1-x}Co_xO$ nanowires in high vacuum as well as in oxygen to investigate the variations in their magnetic properties, and we utilized high-resolution transmission electron microscopy (HRTEM) to inspect the resulting crystal structure of these nanowires. The $Zn_{1-x}Co_xO$ nanowires used in the present work are ∼40 nm in diameter. Various characterization methods, including scanning electron microscopy (SEM), HRTEM, energy dispersive x-ray spectroscopy (EDX), x-ray diffraction (XRD), and electron energy loss spectroscopy (EELS), were carried out to confirm that there does not exist a second phase of Co clusters or any nanocrystal up to the scale of ∼0.5 nm. In other words, to within our experimental limit, there are no aggregations, if any exist at all, containing more than 2–3 Co atoms. The correlations of thermal annealing conditions, structure effects, and O vacancies with the possible occurrence of ferromagnetism in $Zn_{1-x}Co_xO$ nanowires are the main subjects of this work.

This paper is organized as follows. Section 2 describes our experimental method for the fabrication and characterization of 40 nm diameter $Zn_{1-x}Co_xO$ nanowires. Section 3 contains our experimental results and discussion of the various magnetic behaviours of the $Zn_{1-x}Co_xO$ nanowires and their correlations with the structure quality and annealing conditions. Our conclusion is given in section 4.

2. Experimental details

ZnO powder was placed in a crucible situated at the centre of a quartz tube which was placed in a furnace heated to 950 °C. A glass substrate with gold nanoparticles (∼40 nm in diameter) as catalysts pre-deposited on it was located at the downstream end of the quartz tube where the temperature was kept at 500 °C. The chamber was maintained at 200 Pa with a constant flow of argon. After 8 h, ZnO nanowires with an average diameter of ∼40 nm formed on the glass substrate. The as-grown ZnO nanowires were then implanted by 40 keV Co ions with doses of $(1–6)\times10^{16}$ cm^{-2}. The implantation was performed at room temperature by using a tandem accelerator (NEC 9SDH-2). The beam current was kept at 150 nA cm^{-2} to minimize beam heating.

Thermal annealing processes were performed at 600 °C for 12 h. Such an annealing temperature was chosen because it would not lead to any segregation and clustering of Co atoms in the ZnO nanowires, as was confirmed by previous works [33] and our HRTEM studies. Different annealing atmospheres (either an argon flow of 150 sccm at 1 atm or a high vacuum of 5×10^{-5} Torr) were employed to significantly modify the physical properties of the as-implanted $Zn_{1-x}Co_xO$ nanowires. Annealing in an argon flow not only prevented oxidation of the samples but also led to recovering the lattice ordering. On the other hand, annealing in a high vacuum produced oxygen deficiencies and Zn interstitials, and thus possibly changed the carrier concentration in the nanowires. Moreover, a second annealing in 1 atm of either oxygen or argon atmosphere on those already vacuum-annealed samples was also performed for further investigations of the O vacancy effects on ferromagnetism. All the as-implanted and annealed $Zn_{1-x}Co_xO$ nanowires were characterized by using grazing angle XRD (MAC Science, MXP18), field-emission SEM (JEOL JSM-6330F), and HRTEM (JEOL JEM-2010F). EELS and energy loss elemental mapping of nanowires were take by using an EDX system with a Gatan imaging filter. The magnetic properties of the nanowires were measured by using a Quantum Design SQUID magnetometer.

3. Results and discussion

Most of our as-grown ZnO nanowires lay on the substrate. A top-view SEM image of our nanowires on a glass substrate as schematically displayed in figure 1(a) shows that the as-grown ZnO nanowires are ∼40 nm in diameter and 2–3 μm in length. Most of the nanowires are fairly straight and they possess a circular cross section. HRTEM was used to examine the crystal structure and atomic columns on a spatial scale down to 0.5 nm. The electron diffraction pattern was used to inspect the periodicity of selected areas. A representative HRTEM image of the as-grown ZnO nanowires

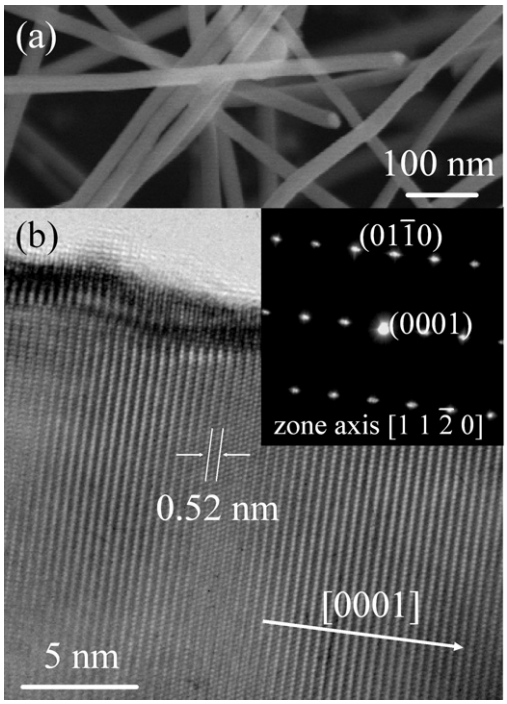

Figure 1. (a) Top-view SEM image of as-grown ZnO nanowires. (b) HRTEM image and its corresponding electron diffraction pattern (inset) displaying the single-crystalline structure of an as-grown ZnO nanowire.

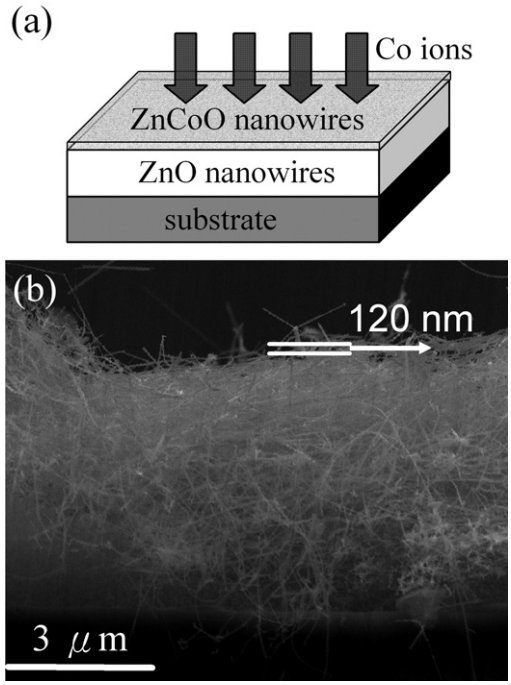

Figure 2. (a) Schematic illustration of the preparation method for Co-implanted ZnO nanowires. (b) Side-view SEM image of ZnO nanowires grown on a glass substrate. The estimated thickness of the thin, as-implanted $Zn_{1-x}Co_xO$ nanowire-formed layer is depicted in the image.

and its corresponding diffraction pattern with zone axis of [11$\bar{2}$0] are shown in figure 1(b). The lattice fringe spacing of 0.52 nm as indicated corresponds to the separation distance between the (001) planes and is in agreement with the lattice constants for the ZnO wurtzite structure. The growth direction of the ZnO nanowire is [0001], and the whole wire comprises a single-crystalline structure.

The as-grown ZnO nanowires were implanted by 40 keV Co ions as depicted in figure 2(a). This implantation process for producing $Zn_{1-x}Co_xO$ nanowires was chosen because it ensured a random and uniform distribution of Co ions in the ZnO matrix. In bulk ZnO, the implanted Co ion distribution estimated from the SRIM simulation [34] predicted a peak at 20 nm and a range of ∼40 nm. The predicted implantation range, which was near the average diameter of our nanowires, guaranteed a uniform distribution of Co ions in the bombarding direction. The Co concentrations in our nanowires were determined from the EDX results, as will be described below and in figure 3. Alternatively, the thickness of the resulted $Zn_{1-x}Co_xO$ nanowire layer can be evaluated in the following manner. We know that the bombardment of a dose of 1×10^{16} cm^{-2} Co ions produced the as-implanted $Zn_{0.98}Co_{0.02}O$ nanowires. By assuming all Co ions were implanted in the ZnO matrix without loss, we estimated the thickness of this layer to be ∼120 nm. This evaluated thickness is ∼3 times as large as the implanted Co ion range inferred from the SRIM code simulation. Such a discrepancy could readily result from the geometrical difference between a bulk and a nanowire-formed layer. The whole layer of the ZnO nanowire with a thickness of 4–5 μm covered with a very thin $Zn_{1-x}Co_xO$ nanowire layer of ∼120 nm is shown in the side-view SEM image in figure 2(b).

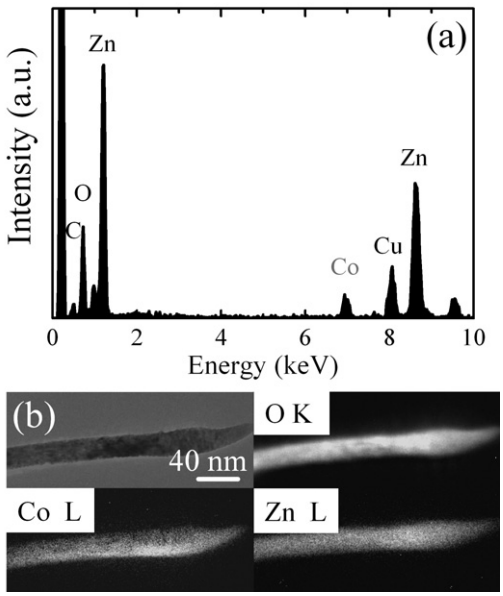

Figure 3. (a) EDX spectroscopy of the as-implanted $Zn_{0.89}Co_{0.11}O$ nanowires. (b) Bright-field image of the as-implanted $Zn_{0.89}Co_{0.11}O$ nanowires with compositional EELS mapping of the O K edge, Co L edge and Zn L edge.

The Co concentration of the as-implanted $Zn_{1-x}Co_xO$ nanowires was determined from the relative ratio of the Co element among Zn and O elements by using EDX spectroscopy. Measurements on more than 20 different nanowires from the same Co ion-dosed sample were carried

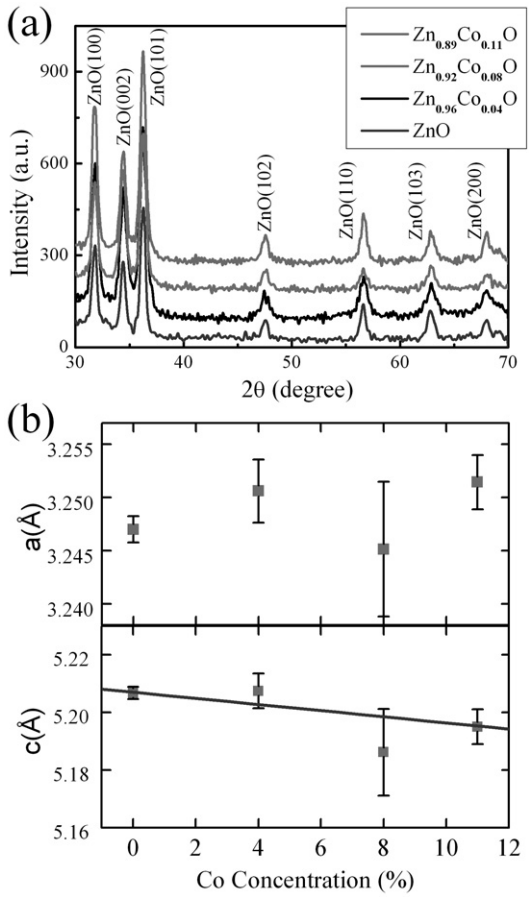

Figure 4. (a) Room-temperature x-ray diffraction patterns for the as-grown ZnO nanowires and the as-implanted $Zn_{1-x}Co_xO$ nanowires as indicated. (b) Variation of the a-axis and c-axis lattice constants with Co concentration x.

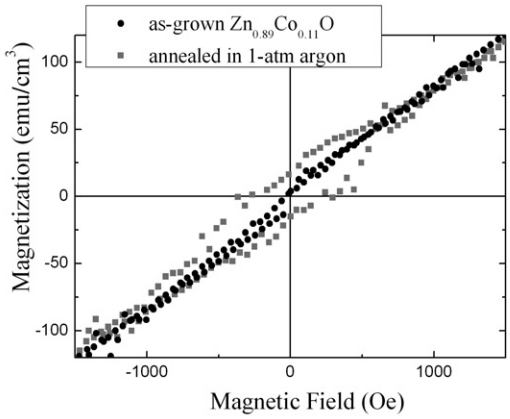

Figure 5. Hysteresis loops of the $Zn_{0.89}Co_{0.11}O$ nanowires before and after annealing in 1 atm argon flow. The data were taken at 2 K.

out to determine the x value. A typical EDX spectrum of the as-implanted $Zn_{0.89}Co_{0.11}O$ nanowire is shown in figure 3(a). The peaks indicating C and Cu elements came from the background of the copper grid used in the HRTEM measurement. A quantitative analysis of the integrated area in the EDX spectrum reveals the atomic ratio of 11% of Co. The average x values are $4.2 \pm 0.9\%$, $7.9 \pm 1.6\%$, and $11.0 \pm 1.8\%$ for $Zn_{1-x}Co_xO$ nanowires with doses of 2, 4, and 6×10^{16} cm^{-2} Co ions, respectively. These x values determined from the EDX results revealed a fairly linear dependence on the Co doses. Thus, we have approximated the average x values to be 2, 4, 6, 8, 10, and 11 at.% in our samples dosed with 1, 2, 3, 4, 5, and 6×10^{16} cm^{-2} Co ions, respectively. The spatial resolution limit of the EDX mapping as was described in our previous work [33] is about 4 nm. The compositional EELS map of the same $Zn_{0.89}Co_{0.11}O$ nanowire is displayed in figure 3(b). The bright-field zero-loss EELS mapping with the corresponding image of Co L edge exhibits a uniform distribution of the Co element in the ZnO nanowire. The images of the O K and Zn L edges are also shown in figure 3(b) to confirm the data of the EELS map. In the image of the Co L edge, no Co clusters or nanocrystals were found within the spatial resolution limit of about 1.8 nm [35].

The crystal structures of the as-grown and the as-implanted ZnO nanowires were characterized by grazing angle XRD patterns, and are shown in figure 4(a). An incident angle of 0.5° was used to observe the crystal structure of the surface layer of $Zn_{1-x}Co_xO$ nanowires. The XRD pattern for the as-grown ZnO nanowires is also plotted for comparison. The XRD data indicate that all the as-implanted $Zn_{1-x}Co_xO$ nanowires are single phased and possess a wurtzite structure. The ZnO nanowires remain crystalline even under the bombardment from our highest dose of 6×10^{16} cm^{-2} Co ions. No perceptible peaks showing any second phases of Co clustering or CoO nanocrystals, as were identified in previous results [36], were found in this work. The spatial resolution limit to detect clusters or nanocrystals from the XRD patterns is about 10 nm. Figure 4(b) shows a small variation of a and c lattice constants for the $Zn_{1-x}Co_xO$ nanowires as a function of the x values. We see that changes in the a-axis lattice constant is minute while a tendency of a slight decrease in the c-axis lattice constant is observed. The decrease in c-axis lattice constant is consistent with previous data of polycrystalline Co-substituted ZnO [21] but is in conflict with data of Co-doped ZnO films prepared by pulsed laser deposition [12].

3.1. Structural effects on ferromagnetism

The magnetic properties of $Zn_{1-x}Co_xO$ nanowires were investigated by using a SQUID magnetometer. All of our as-implanted nanowires displayed paramagnetic behaviour at 2 K. That is, there are no detectable hysteresis loops, indicating the absence of any ferromagnetic ordering. Since the mechanism of FM in DMS materials is still unclear, while it is known that different preparation methods can profoundly alter the magnetic behaviours, we were motivated to investigate the structure effect on ferromagnetism in Co-doped ZnO nanowires in this work. The crystal structures of our nanowires were markedly modified after the Co ion implantation process (see below). Thus, we performed thermal annealing of our nanowires in 1 atm argon to restore the crystal order and then measured the magnetizations as a function of the magnetic field. Noticeably, after the argon annealing, we observed profound hysteresis loops at 2 K in all $Zn_{1-x}Co_xO$ nanowires. The hysteresis loops for the as-implanted (closed circles) and then annealed (closed squares) $Zn_{0.89}Co_{0.11}O$ nanowires are shown in figure 5 for comparison.

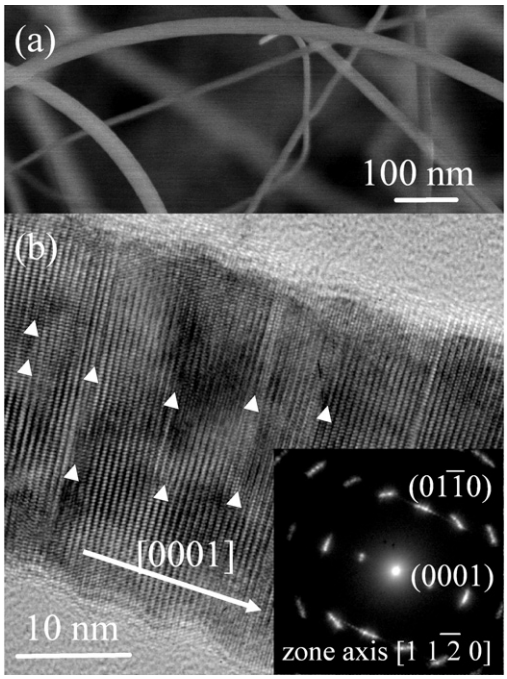

Figure 6. (a) SEM image of as-implanted $Zn_{0.94}Co_{0.06}O$ nanowires. (b) HRTEM image of as-implanted $Zn_{0.89}Co_{0.11}O$ nanowires with white triangles indicating one type of structural defect, i.e., stacking faults. Inset: an electron diffraction pattern revealing another type of structural defect, i.e., orientational variations.

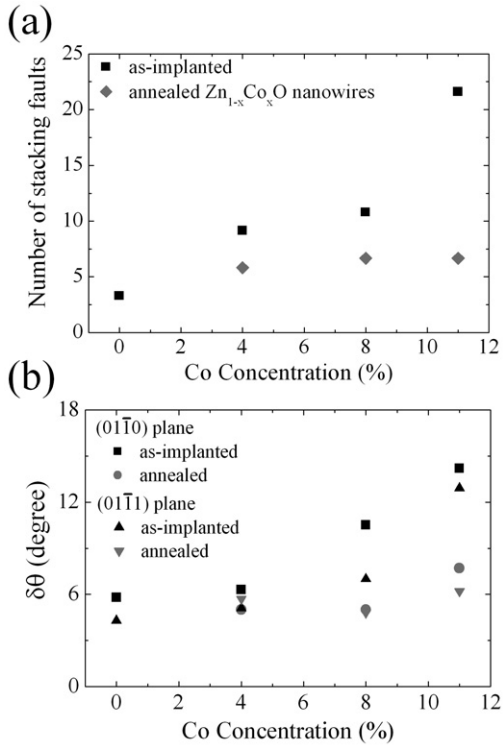

Figure 7. (a) Variation of the number of stacking faults per 100 nm in length along the [0001] growth direction of as-implanted and annealed $Zn_{1-x}Co_xO$ nanowires with the Co concentration. (b) Variation of the deviation angle of the (01$\bar{1}$0) and (01$\bar{1}$1) plane sets along the [11$\bar{2}$0] axis with the Co concentration.

The appearance of hysteresis loops, a characteristic behaviour of FM, points to domain wall motion in our 40 nm diameter $Zn_{1-x}Co_xO$ nanowires. Apart from the nonreversible loops we can see the linear and reversible component in the field-dependent magnetization. The linear part may originate from some isolated Co ions without ferromagnetic exchange interaction with other magnetic cations. To reduce the effect of the linear component from those paramagnetic impurities we used the same sample for subsequent thermal treatments and magnetization measurements.

Bearing in mind investigating the crystal structure effects on the possible occurrence of FM, the $Zn_{1-x}Co_xO$ nanowires, both before and after annealing in argon, were carefully examined by HRTEM. We first show the SEM and HRTEM images of the as-implanted nanowires in figure 6. Right after ion implantation but before argon annealing, the morphology and dimensions of the $Zn_{1-x}Co_xO$ nanowires did not change appreciably, except a bending of the nanowires occurred. The HRTEM image shows a single-crystalline structure with a [0001] growth direction (which is the growth direction for our as-grown ZnO nanowires). The bending effect could also be observed in the [11$\bar{2}$0] electron diffraction pattern, as shown in the inset of figure 6(b) for the as-implanted $Zn_{0.89}Co_{0.11}O$ nanowires. A small rotation with respect to the zone axis generated deviation angles for the (01$\bar{1}$0) and (01$\bar{1}$1) plane sets. The first type of structural defect (called orientational variations) exhibited bending in the SEM image and rotation of plane-set points in the selected area electron diffraction pattern. A second type of structural defect (called stacking faults) was also found, as indicated by the many small triangles in the HRTEM image shown in figure 6(b). The locations of the small triangles marking stacking faults were determined from the back and forth fast Fourier transform analysis of the (0001) plane set.

We have quantitatively analysed these two types of structural defect in our nanowires as described below. The numbers of stacking faults in the as-grown ZnO and the as-implanted $Zn_{1-x}Co_xO$ nanowires were counted per 100 nm in length along the [0001] direction and are plotted as a function of Co concentration in figure 7(a). The number of stacking faults for each Co concentration was evaluated and averaged by counting over 20 $Zn_{1-x}Co_xO$ nanowires. For comparison, the amount of stacking faults in the as-grown ZnO nanowires is also plotted. We found that the Co ion implantation generates a good number of stacking faults. Some of the stacking faults were, however, removed by the thermal annealing process. After 1 atm argon annealing, the number of stacking faults was reduced to the level of 6–7 per 100 nm in length, which was still twice that in the as-grown ZnO nanowires. In particular, the crystalline structure of the $Zn_{1-x}Co_xO$ nanowires was now greatly recovered.

The slight bending of the as-implanted $Zn_{1-x}Co_xO$ nanowires was quantified by deviation angles representing the rotation of plane-set points in the electron diffraction pattern. Figure 7(b) shows the deviation angles in degrees as a function of the Co concentration for both the as-implanted and annealed $Zn_{1-x}Co_xO$ nanowires. We see that the deviation angles for the plane sets of (01$\bar{1}$0) and (01$\bar{1}$1) changed by a factor of ∼2 in the as-implanted nanowires, as compared with those in the

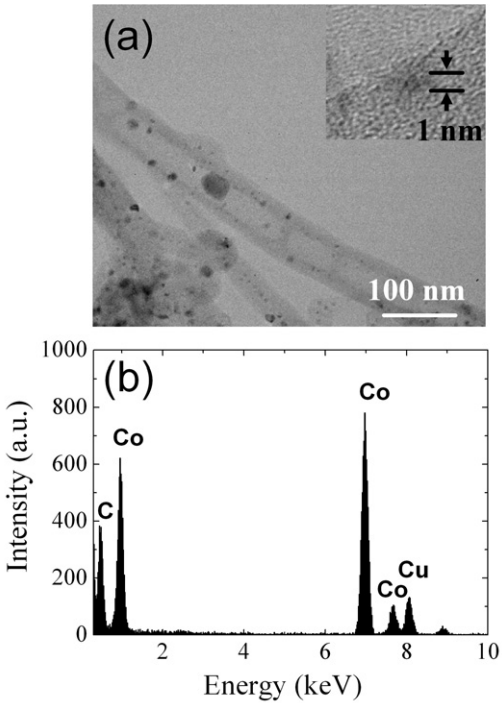

Figure 8. (a) TEM image of Co clusters on surfaces of carbon-coated ZnO nanowires. Inset: HRTEM image of a Co cluster. (b) EDX spectroscopy of a Co cluster on the surface of carbon-coated ZnO nanowires.

annealed nanowires. On the other hand, the deviation angle was barely changed for the (0001) plane set. We notice that the argon annealing is much more effective in removing stacking faults than orientation variations. This result suggests that the structure defects due to stacking faults are more detrimental to the occurrence of FM in the as-implanted $Zn_{1-x}Co_xO$ nanowires, as compared with the structural defects due to orientational variations. We also notice that the lattice planes along the [0001] direction are fairly well ordered even after ion bombardment, while those planes in other directions are more disordered.

In addition to the quantitative analysis discussed above, we carefully examined the microstructures of the as-implanted and the annealed $Zn_{1-x}Co_xO$ nanowires from the HRTEM images and the electron diffraction patterns. We found no sign of a second phase due to either Co clustering or CoO nanocrystals in the HRTEM images. Also, no extra diffraction spots other than those characteristic to ZnO have ever been detected from the electron diffraction patterns. Moreover, in order to provide further clarifications, we purposely fabricated carbon-coated ZnO nanowires, as shown in figure 8(a), and then performed Co ion implantation and high-vacuum annealing. In this case, we clearly observed Co metal clustering on the surfaces of the carbon-coated ZnO nanowires. A typical HRTEM image of a 1 nm Co cluster is also shown in the inset of figure 8(a). The dotted microstructures observed in HRTEM images were determined to consist of Co atoms, without O element, by using EDX analysis (see figure 8(b)). It should be stressed that when we examined our $Zn_{1-x}Co_xO$ nanowires without carbon coating, we did not find any similar Co clustering on the surfaces.

Our results are consistent with a previous report [37] that the implantation defects were removed upon the annealing procedure and that the annealing does not result into an out-diffusion of magnetic cations. Besides, the results agree well with the concept that a uniform distribution of Co ions in ZnO host favours FM ordering [38, 26]. It may imply an absence of FM in some polycrystalline samples [39, 40]. Although a theoretical argument exists that the structural optimization has little effect on the couplings for $Zn_{1-x}Co_xO$ [27], we believe that the crystallinity is crucial for turning on the FM.

3.2. Annealing effects on ferromagnetism

We studied the structure effects on the ferromagnetic ordering through measuring the hysteresis loops in the $Zn_{1-x}Co_xO$ nanowires both before and after annealing in an argon flow. Our results for the structure effects provide important clue for resolving the controversial issue of whether ferromagnetic ordering could occur in crystalline and polycrystalline Co-substituted ZnO [12, 21]. However, as mentioned in the Introduction, ZnO is very sensitive to the ambient air as well as the partial pressure of oxygen. Therefore, we also performed the annealing in a high vacuum of 5×10^{-5} Torr and studied the magnetizations of the $Zn_{1-x}Co_xO$ nanowires. Furthermore, we then performed a second annealing on those already vacuum-annealed nanowires in either an argon or oxygen atmosphere for further investigations of their magnetic properties.

Our measured hysteresis loops for both the argon- and vacuum-annealed $Zn_{1-x}Co_xO$ nanowires are presented in figure 9(a). The hysteresis loops are much more profound for the $x = 0.11$ nanowires relative to the $x = 0.08$ nanowires, clearly demonstrating the formation of enhanced ferromagnetic domains when more Co ions are introduced into the ZnO nanowires. Inspection of figure 9(a) reveals that much stronger FM is found in the vacuum-annealed $Zn_{1-x}Co_xO$ nanowires, while the argon-annealed nanowires revealed weaker FM. From the HRTEM and diffraction pattern analysis, we found that the crystal structure of the vacuum-annealed nanowires reveals no discernible difference from that of the argon-annealed nanowires. Therefore, we believe that another mechanism in addition to the structure effects must contribute to the striking enhancement of FM in the Co-implanted ZnO. Figure 9(b) shows a plot of the temperature dependencies of the magnetizations for the vacuum-annealed $Zn_{1-x}Co_xO$ nanowires. Noticeably, the magnetization of the vacuum-annealed nanowires still displays clear hysteresis loops at 10 K (as a matter of fact, a hysteresis loop can even be observed at room temperature, not shown). On the other hand, we point out that the hysteresis loops for the argon-annealed $Zn_{1-x}Co_xO$ nanowires quickly diminished with increasing temperature and totally disappeared above 10 K.

In order to investigate the possible mechanism for the occurrence of enhanced FM in the high-vacuum annealed $Zn_{1-x}Co_xO$ nanowires, we also performed a subsequent second annealing in either an argon or oxygen atmosphere on those vacuum-annealed samples. We found that, after a second annealing in 1 atm *argon*, both the temperature and magnetic field behaviours of the magnetizations are unchanged. However, if the second annealing is performed in an *oxygen* atmosphere, the hysteresis loop for the nanowires

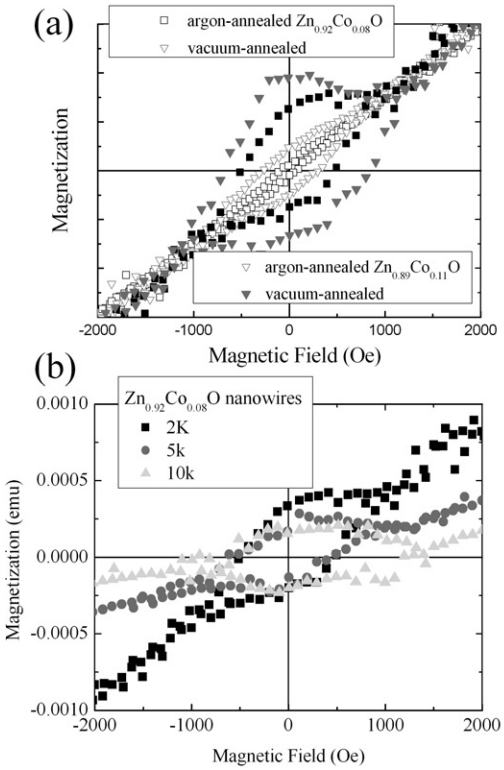

Figure 9. (a) Hysteresis loops for argon-annealed and high-vacuum annealed $Zn_{0.92}Co_{0.08}O$ and $Zn_{0.89}Co_{0.11}O$ nanowires at 2 K. The magnetization was normalized to that at the field of 1500 Oe for comparison. (b) Hysteresis loops for the high-vacuum annealed $Zn_{0.92}Co_{0.08}O$ nanowires at 2, 5, and 10 K as indicated.

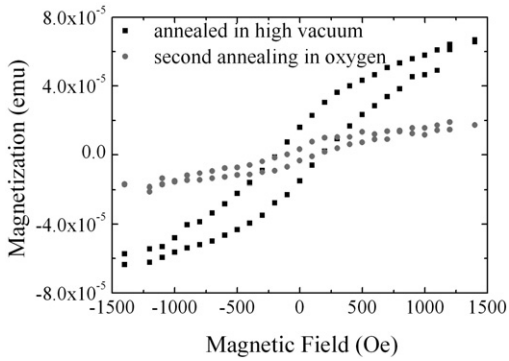

Figure 10. Hysteresis loops for the same $Zn_{0.89}Co_{0.11}O$ nanowires after a first annealing in high vacuum and then a second annealing in oxygen. The data were taken at 2 K.

greatly diminishes and the magnetization is notably attenuated (see figure 10). The diminished FM in the vacuum-annealed $Zn_{1-x}Co_xO$ nanowires followed with an oxygen annealing immediately implies a decisive role being played by O element in determining the magnetic properties of the nanowires. We believe that the first high-vacuum annealing results in the formation of a good number of O vacancies in the nanowires, while the second annealing in oxygen largely fills those vacancies up again with O. It is established that ZnO is a native n-type material with the dopants generating from either O vacancies or Zn interstitials [41]. Consequently, we may draw the conclusion that the enhanced FM found in the vacuum-annealed nanowires is very likely caused by a change in the electron concentration due to the generation of a large amount of O vacancies. We cannot inspect point defects of O vacancies but can observe planar defects of stacking faults through HRTEM analysis. Taking the results from second annealing together, we conclude that the effect of argon annealing is mainly to remove structure defects only, while high-vacuum annealing causes an extra effect of increasing the number of O vacancies in ZnO.

To trace the origin of the enhanced FM found in the high-vacuum annealed nanowires, we carried out measurements of EELS spectra in the as-implanted, argon-annealed, and high-vacuum annealed $Zn_{1-x}Co_xO$ nanowires. The technique of L_3/L_2 intensity ratio correlating the EELS spectra with the valence states [42, 43] was used to determine the change of the oxidation state of Co ions in our nanowires. To determine the numerical ratio of L_3/L_2, a double arctangent function was used as a background function for subtracting the background intensity. The intensity ratios thus determined for the as-implanted, argon-annealed, and vacuum-annealed $Zn_{1-x}Co_xO$ nanowires are 3.5, 3.4, and 3.1, respectively. We see that the valence state of Co ions in the argon-annealed nanowires is barely changed from that in the as-implanted nanowires.

The results of annealing effects, pointing out the important roles played by defects, are consistent with recent observation of reversible 300 K FM ordering in Co^{2+}:ZnO thin film [44] and thin film grown by ultrasonic-assisted solution chemical vapour deposition [45]. Double-exchange mechanisms [46] from either Zn interstitials or O vacancies in our observations are theoretically supported [29, 27], and it will thus provide adequate description of the FM in the $Zn_{1-x}Co_xO$ system.

4. Summary

In this work, we fabricated $Zn_{1-x}Co_xO$ nanowires by using the standard ion implantation technique. The Co ions were uniformly distributed in nanowires, as was inspected by using EELS map under a spatial resolution of ∼1.8 nm. In addition, no second phase of either Co clustering or CoO nanocrystals was found in the nanowires by using HRTEM within our spatial resolution of ∼0.5 nm. The c lattice constant of the $Zn_{1-x}Co_xO$ nanowires decreases with increasing Co concentration x. The as-implanted nanowires showed no sign of ferromagnetic ordering at 2 K. In the as-implanted $Zn_{1-x}Co_xO$ nanowires, two types of structural defect (i.e., stacking faults and orientational variations) were found. After annealing in argon, the removal of structural defects and the recovery of structure order introduced FM in the $Zn_{1-x}Co_xO$ nanowires, which displayed noticeable hysteresis loops up to 10 K. We found that the structure defects due to stacking faults are more detrimental to the occurrence of FM. For comparison, we performed Co implantation on carbon-coated ZnO nanowires and found clear Co clusters in HRTEM images. Most noticeably, thermal annealing in high vacuum caused a largely enhanced FM ordering in the $Zn_{1-x}Co_xO$ nanowires. A subsequent second annealing on the vacuum-annealed nanowires was performed to illustrate that O vacancies play decisive roles in determining the occurrence of ferromagnetism. EELS spectra revealed a slight shift toward a

higher oxidation state for Co ions in the high-vacuum annealed nanowires, relative to that in the as-implanted and the argon-annealed $Zn_{1-x}Co_xO$ nanowires.

Acknowledgments

This work was supported by the National Science Council of ROC under Grant Nos NSC 93-2112-M-009-038, NSC 93-2120-M-009-009 and NSC 94-2120-M-009-010, and by the MOE ATU Program.

References

[1] Furdyna J K 1988 *J. Appl. Phys.* **64** R29
[2] Wolf S A, Awschalom D D, Buhrman R A, Daughton J M, von Molnár S, Roukes M L, Chtchelkanova A Y and Treger D M 2001 *Science* **294** 1488
[3] Story T, Galazka R R, Frankel R B and Wolff P A 1986 *Phys. Rev. Lett.* **56** 777
[4] Munekata H, Ohno H, von Molnar S, Segmüller A, Chang L L and Esaki L 1989 *Phys. Rev. Lett.* **63** 1849
[5] Ohno H, Shen A, Matsukura F, Oiwa A, Endo A, Katsumoto S and Iye Y 1996 *Appl. Phys. Lett.* **69** 363
[6] Matsukura F, Ohno H, Shen A and Sugawara Y 1998 *Phys. Rev.* B **57** R2037
[7] Dietl T, Ohno H, Matsukura F, Cibert J and Ferrand D 2000 *Science* **287** 1019
[8] Heo Y W, Park S J, Ip K, Pearton S J and Norton D P 2003 *Appl. Phys. Lett.* **83** 1128
[9] Li Z Q, Zhang D X and Lin J J 2006 *J. Appl. Phys.* **99** 124906
[10] Huang M H, Mao S, Feick H, Yan H, Wu Y, Kind H, Weber E, Russo R and Yang P 2001 *Science* **292** 1897
[11] Heo Y W, Norton D P, Tien L C, Kwon Y, Kang B S, Ren F, Pearton S J and LaRoche J R 2004 *Mater. Sci. Eng.* R **47** 1
[12] Ueda K, Tabata H and Kawai T 2001 *Appl. Phys. Lett.* **79** 988
[13] Lee H J, Jeong S Y, Cho C R and Park C H 2002 *Appl. Phys. Lett.* **81** 4020
[14] Rode K, Anane A, Mattana R, Contour J P, Durand O and LeBourgeois R 2003 *J. Appl. Phys.* **93** 7676
[15] Prellier W, Fouchet A, Mercey B, Simon C and Raveau B 2003 *Appl. Phys. Lett.* **82** 3490
[16] Ramachandran S, Tiwari A and Narayan J 2004 *Appl. Phys. Lett.* **84** 5255
[17] Wu J J, Liu S C and Yang M H 2004 *Appl. Phys. Lett.* **85** 1027
[18] Kittilstved K R, Norberg N S and Gamelin D R 2005 *Phys. Rev. Lett.* **94** 147209
[19] Chen J J, Yu M H, Zhou W L, Sun K and Wang L M 2005 *Appl. Phys. Lett.* **87** 173119
[20] Sati P *et al* 2006 *Phys. Rev. Lett.* **96** 017203
[21] Risbud A S, Spaldin N A, Chen Z Q, Stemmer S and Seshadri R 2003 *Phys. Rev.* B **68** 205202
[22] Kobayashi M *et al* 2005 *Phys. Rev.* B **72** 201201
[23] Wi S C *et al* 2004 *Appl. Phys. Lett.* **84** 4233
[24] Norton D P *et al* 2003 *Appl. Phys. Lett.* **83** 5488
[25] Park J H, Kim M G, Jang H M, Ryu S and Kim Y M 2004 *Appl. Phys. Lett.* **84** 1338
[26] Martinez B, Sandiumenge F, Balcells L, Arbiol J, Sibieude F and Monty C 2005 *Appl. Phys. Lett.* **86** 103113
[27] Sluiter M H F, Kawazoe Y, Sharma P, Inoue A, Raju A R, Rout C and Waghmare U V 2005 *Phys. Rev. Lett.* **94** 187204
[28] Petit L, Schulthess T C, Svane A, Szotek Z, Temmerman W M and Janotti A 2006 *Phys. Rev.* B **73** 045107
[29] Coey J M D, Venkatesan M and Fitzgerald C B 2005 *Nat. Mater.* **4** 173
[30] Sato K and Katayama-Yoshida H 2001 *Japan. J. Appl. Phys.* **40** L334
[31] Venkatesan M, Fitzgerald C B, Lunney J G and Coey J M D 2004 *Phys. Rev. Lett.* **93** 177206
[32] Spaldin N A 2004 *Phys. Rev.* B **69** 125201
[33] Jian W B, Wu Z Y, Huang R T, Chen F R, Kai J J, Wu C Y, Chiang S J, Lan M D and Lin J J 2006 *Phys. Rev.* B **73** 233308
[34] Ziegler J F and Biersak J P http://www.srim.org
[35] Egerton R F and Crozier P A 1997 *Micron* **28** 117
[36] Kolesnik S, Dabrowski B and Mais J 2004 *J. Appl. Phys.* **95** 2582
[37] Ronning C, Gao P X, Ding Y, Wang Z L and Schwen D 2004 *Appl. Phys. Lett.* **84** 783
[38] Martinez B, Sandiumenge F, Balcells Ll, Arbiol J, Sibieude F and Monty C 2005 *Phys. Rev.* B **72** 165202
[39] Lawes G, Risbud A S, Ramirez A P and Seshadri R 2005 *Phys. Rev.* B **71** 045201
[40] Bouloudenine M, Viart N, Colis S, Kortus J and Dinia A 2005 *Appl. Phys. Lett.* **87** 052501
[41] Look D C, Hemsky J W and Sizelove J R 1999 *Phys. Rev. Lett.* **82** 2552
[42] Wang Z L, Yin J S and Jiang Y D 2000 *Micron* **31** 571
[43] Pearson D H, Fultz B and Ahn C C 1988 *Appl. Phys. Lett.* **53** 1405
[44] Schwartz D A and Gamelin D R 2004 *Adv. Mater.* **16** 2115
[45] Khare N, Kappers M J, Wei M, Blamire M G and MacManus-Driscoll J L 2006 *Adv. Mater.* **18** 1449
[46] García M A *et al* 2005 *Phys. Rev. Lett.* **94** 217206